Cross-RIS-Aware Phase Design for Multi-cell Multi-RIS Networks

Sungyun Oh
Dept. Electronics and Information Engineering
Korea University
Sejong, Republic of Korea
2019270745@korea.ac.kr

Heejung Yu
Dept. Electronics and Information Engineering
Korea University
Sejong, Republic of Korea
heejungyu@korea.ac.kr

***Abstract*—Reconfigurable intelligence surfaces (RISs) have emerged as an efficient technology to enhance the spectral and energy efficiency of wireless networks. Most existing RIS studies have adopted an ideal phase-shift model under a narrow-band assumption and designed the RIS phases selfishly to maximize the rate of each cell, ignoring reflections paths via neighboring-cell RISs that operate on different frequencies. In this paper, we studied the RIS-aided multi-cell wireless system. Specifically, for a two-cell downlink at two different center-frequencies, we consider a practical (frequency-selective, i.e, wide-band) model and explicitly account for other-cell RIS, i.e., cross-RIS, reflections. We formulate a new optimization problem of designing a common RIS phase shift, jointly considering the two BS signals at the RIS to maximize the average rate of two users. We also evaluate sensitivity to the codebook size for quantized phases and compared against a self-RIS baseline. The proposed design yields higher average rate across the two users, offering insights for the use of neighboring-cell RIS in next-generation networks.**

I. Introduction

Reconfigurable intelligence surfaces (RISs) have emerged as a cost-effective approach to enhance the spectral and energy efficiency of wireless networks [1]–[11]. Previous studies have developed energy-efficient schemes that jointly optimize the base-station(BS) transmit power and the RIS phase shifts, using alternating maximization with gradient-based phase updates and fractional programming [12]. Most of the previous studies adopt ideal, frequency-flat phase-shift models [13] or optimize RIS phases on a self-RIS link basis, effectively ignoring reflections routed through neighboring RIS. These assumptions become questionable in wide-band deployments and in multi-cell settings where adjacent cells operate at different center frequencies. This paper suggests an RIS phase-shift design in a wide-band network system. We consider a two-cell down-link in which two BSs operate at adjacent bands, each assisted by an RIS. In wide-band systems where transmit signals have different center frequencies, e.g., two BS assign different frequency resources to users severed simultaneously in RIS-aided orthogonal frequency division multiple access (OFDMA) systems. Under such a network configuration, RIS phase shifts should be designed carefully by considering the actual phase-shift depending on the carrier frequency [14]. Some studies shows that an RIS optimized and controlled by one base station can significantly improve the communication rate of another operator using a different frequency band, even though the other BS has no control over the RIS. From the perspective of the out-of-band user, the RIS phases appear completely random. Nevertheless, the additional signal paths introduced by the RIS consistently enhance performance, leading to measurable rate and signal-to-noise ratio (SNR) gains [15]. Following this study, we formulate a cross-RIS-aware phase-shift design problem that maximizes the network average sum rate by explicitly accounting for cross-RIS reflections. We solve this problem via a block coordinate ascent (BCA) algorithm. In each sweep, i.e., iteration, all RIS elements are updated sequentially with continuous phase values, which are subsequently quantized to the nearest point in a finite-bit quantized code-book. Since the updates are performed sequentially, later updates implicitly revise the overall configuration, and then we report the convergence behavior in terms of the average sum rate versus the number of sweeps (i.e., iterations).

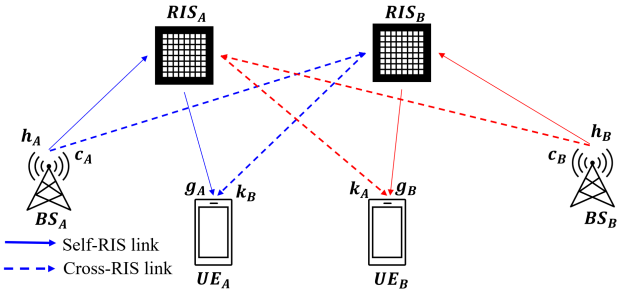

Fig. 1. RIS-aided multi-cell multi-user networks.

II. System model

As shown in Fig. 1, we consider a two-cell down-link in which two BSs, i.e., BS_A and BS_B, operate at 2.4 and 2.5 GHz with 100 MHz bandwidth and K subcarriers, respectively, each assisted by an RIS (RIS_A and RIS_B) with N reflecting elements. Because two cells are overlapped, there can exist multiple signal paths as in Fig. 1, where solid lines denote self-RIS paths, and dashed lines denote cross-RIS paths. The RIS phase shifts must be designed on a per-subcarrier basis, as wide-band frequency selectivity entails different center

frequencies across subcarriers. The relation between the center frequency and the phase design is detailed in [16].

A. Channel Model

We adopt a wide-band free-space model. The transmit power for each BS_A, BS_B is denoted as P_A, P_B. With K subcarriers and N RIS reflecting elements, the corresponding channel vectors are defined as illustrated in Fig. 1. The self-RIS path from BS_A (BS_B) to RIS_A (RIS_B) on the kth subcarrier is denoted by $\boldsymbol{h}_{A,k}$ ($\boldsymbol{h}_{B,k}$). The self-RIS reflecting path from RIS_A (RIS_B) to UE_A (UE_B) on the kth subcarrier is denoted by $\boldsymbol{g}_{A,k}$ ($\boldsymbol{g}_{B,k}$). Similarly, the cross-RIS path from BS_A (BS_B) to RIS_B (RIS_A) on the kth subcarrier is denoted by $\boldsymbol{c}_{A,k}$ ($\boldsymbol{c}_{B,k}$). Finally, the croess-RIS reflecting path from RIS_A (RIS_B) to UE_B (UE_A) on the kth subcarrier is denoted by $\boldsymbol{k}_{A,k}$ ($\boldsymbol{k}_{B,k}$). For $i \in \{A, B\}$, we define the BS–RIS and RIS–UE channel vectors on kth subcarrier, considering N reflecting elements as

$$\boldsymbol{h}_{i,k} = [h_{i,k,1}, \ldots, h_{i,k,N}]^T, \tag{1}$$

$$\boldsymbol{g}_{i,k} = [g_{i,k,1}, \ldots, g_{i,k,N}]^T, \tag{2}$$

and the cross-RIS channel vectors on kth subcarrier as

$$\boldsymbol{c}_{i,k} = [c_{i,k,1}, \ldots, c_{i,k,N}]^T, \tag{3}$$

$$\boldsymbol{k}_{i,k} = [k_{i,k,1}, \ldots, k_{i,k,N}]^T. \tag{4}$$

We define the RIS reflection-coefficient matrix for RIS_i on the kth subcarrier as follows:

$$\boldsymbol{\Phi}_{i,k} \triangleq \mathrm{diag}(\phi_{i,k,1}, \ldots, \phi_{i,k,n}, \ldots, \phi_{i,k,N}), \tag{5}$$

for $i \in \{A, B\}$. The reflection coefficient of the nth RIS element on kth subcarrier, i.e., $\phi_{i,k,n}$, is written as

$$\phi_{i,k,n} = A_{i,k,n} e^{j\theta_{i,k,n}}, \tag{6}$$

where $A_{i,k,n}$ and $\theta_{i,k,n}$ denote the amplitude and phase of the nth element on kth subcarrier of RIS_i, respectively. The received signals at UE_A and UE_B on kth subcarrier are given by

$$y_{A,k} = \sqrt{P_A}\Big(\boldsymbol{g}_{A,k}^T \boldsymbol{\Phi}_{A,k} \boldsymbol{h}_{A,k} + \boldsymbol{k}_{B,k}^T \boldsymbol{\Phi}_{B,k} \boldsymbol{c}_{A,k}\Big) x_{A,k} + n_{A,k}. \tag{7}$$

$$y_{B,k} = \sqrt{P_B}\Big(\boldsymbol{g}_{B,k}^T \boldsymbol{\Phi}_{B,k} \boldsymbol{h}_{B,k} + \boldsymbol{k}_{A,k}^T \boldsymbol{\Phi}_{A,k} \boldsymbol{c}_{B,k}\Big) x_{B,k} + n_{B,k}. \tag{8}$$

where $x_{A,k}$ ($x_{B,k}$) with $|x_{A,k}| = 1$ ($|x_{B,k}| = 1$) is the symbol transmitted from BS_A (BS_B) for each subcarrier. $n_{A,k} \sim \mathcal{CN}(0, \sigma^2)$ and $n_{B,k} \sim \mathcal{CN}(0, \sigma^2)$ are additive white Gaussian noise (AWGN) terms. We adopt a free-space (Friis) large-scale model, and all links are assumed to operate in the far field. The small-scale fading terms are modeled as circularly symmetric complex Gaussian random variables with zero mean and variance determined by the corresponding large-scale gain

$$\beta(d, f) = \left(\frac{\lambda}{4\pi d}\right)^2, \quad \lambda = \frac{c}{f_0} \tag{9}$$

where d denotes the distance between a transmitter and receiver, f_0 denotes the carrier frequency. In detail, distances for each channel are given by $d_h = 50\,\mathrm{m}$, $d_g = 70\,\mathrm{m}$, $d_c = 120\,\mathrm{m}$, and $d_k = 90\,\mathrm{m}$, respectively. For each subcarrier k, the $N \times 1$ channel vectors are modeled as

$$\boldsymbol{h}_{i,k} \sim \mathcal{CN}(\boldsymbol{0}, \beta_h \mathbf{I}_N), \tag{10}$$

$$\boldsymbol{g}_{i,k} \sim \mathcal{CN}(\boldsymbol{0}, \beta_g \mathbf{I}_N), \tag{11}$$

$$\boldsymbol{c}_{i,k} \sim \mathcal{CN}(\boldsymbol{0}, \beta_c \mathbf{I}_N), \tag{12}$$

$$\boldsymbol{k}_{i,k} \sim \mathcal{CN}(\boldsymbol{0}, \beta_k \mathbf{I}_N), \tag{13}$$

where the path loss is assumed to be identical for all subcarriers. That is, we neglect the frequency variation across subcarriers and model the each path loss as follows:

$$\beta_h = \beta(d_h, f_0), \tag{14}$$

$$\beta_g = \beta(d_g, f_0), \tag{15}$$

$$\beta_c = \beta(d_c, f_0), \tag{16}$$

$$\beta_k = \beta(d_k, f_0). \tag{17}$$

B. RIS Phase and Amplitude Models

As in [16], the phase shift $\theta_n(\angle\phi_c, f_k)$ and amplitude $A_n(\angle\phi_c, f_k)$, of each RIS element on the kth subcarrier were modeled as function of $\angle\phi_c$ and f_k where $\angle\phi_c$ is the desired phase control input at the center frequency f_0. Please note that the actual phase shift ($\theta_n(\angle\phi_c, f_k)$) for the kth subcarrier can be different from the desired phase control input ($\angle\phi_c$) because the frequency different between the center frequency (f_c) and the frequency of the kth subcarrier (f_k), i.e., $f_k - f_0$. Similarly, the amplitude $A_n(\angle\phi_c, f_k)$, of each RIS element on the kth subcarrier varies depending on the actual frequency of each subcarrier. Since we are dealing with BS_i and kth subcarrier, f_k, we adopt the following parametric model as follows:

$$\theta_{i,k,n}(\angle\phi_{i,c,n}, f_k), \tag{18}$$

$$A_{i,k,n}(\angle\phi_{i,c,n}, f_k), \tag{19}$$

where $\angle\phi_{i,c,n}$ denotes the desired phase control input of the nth element of RIS_i at the center frequency f_0. The detail formulas for phase and amplitude functions can be expressed as [16]:

$$\theta_{i,k,n} = -2\tan^{-1}\left[\mathcal{F}_2\big(\angle\phi_{i,c,n}\big)\left(\frac{f_k}{10^9} - \mathcal{F}_1\big(\angle\phi_{i,c,n}\big)\right)\right], \tag{20}$$

$$A_{i,k,n} = -\frac{\alpha_4 \angle\phi_{i,c,n} + \beta_3}{\left(\left(f_k - \mathcal{F}_1\left(\angle\phi_{i,c,n}\right)\right)/0.05\right)^2 + 4} + 1, \tag{21}$$

where

$$\mathcal{F}_1(\angle\phi_{i,c,n}) = \alpha_1 \tan(\angle\phi_{i,c,n}/3) + \alpha_2 \sin\big(\angle\phi_{i,c,n}\big) + \beta_1,$$
$$\mathcal{F}_2(\angle\phi_{i,c,n}) = \alpha_3 \angle\phi_{i,c,n} + \beta_2, \tag{22}$$

for $n = \{1, \ldots, N\}$. Here, $\{\alpha_i\}$ and $\{\beta_i\}$ are fitting parameters obtained from the hardware measurements (see Table I). For detailed expressions, refer to [16].

TABLE I
PARAMETERS IN (21) AND (22) AT EACH CENTER FREQUENCY.

Center Frequency	α_i				β_i		
	α_1	α_2	α_3	α_4	β_1	β_2	β_3
2.4 GHz	0.2	-0.015	-0.75	-0.05	2.4	11.02	1.65
2.5 GHz	0.299	-0.073	-0.641	-0.078	2.51	9.973	1.926

III. Optimal RIS Control in Multi-cell Multi-RIS Networks

As discussed in the previous section, the actual RIS phase shift of the wideband signal can be unintentionally determined due to frequency difference between subcarrier frequency f_k and the center frequency f_0. This is similar to the bean squint effect in the widebank beamforming. Additionally, the transmitted signal by one BS can be unintentionally reflected by RISs in the neighboring cells. This unintentional reflection may increase the signal power. If the reflected path via other cell RISs is properly exploited, the additional performance improvement can be obtained. To maximize the performance gain with multiple RISs in multiple cells, the cooperation between BSs are required. In this section, we proposed two different RIS control policies, i.e., selfish and cross-RIS-aware mechanisms, are investigated.

A. Case-1: Selfish RIS Control

As shown in Fig.1, *Case-1* considers only the signal reflected by the own cell's RIS, i.e., neglecting the RIS in the other cell. Therefore, each BS (BS_i) controls an RIS in the own cell (RIS_i) to maximize the achievable rate at UE_i for $i \in \{A, B\}$. Therefore, the objective function, i.e., achievable rate of UE_i, can be expressed by

$$R_i = \frac{1}{K}\sum_{k=1}^{K}\log_2\left(1+\frac{P_i\left|H_{i,k}\right|^2}{\sigma^2}\right) \tag{23}$$

where the effective channel gain from BS_i to UE_i via RIS_i is defined by $H_{i,k}$. Therefore, $H_{i,k}$'s for $i \in \{A, B\}$ are given by $H_{A,k} \triangleq \boldsymbol{g}_{A,k}^T \boldsymbol{\Phi}_{A,k} \boldsymbol{h}_{A,k}$ and $H_{B,k} \triangleq \boldsymbol{g}_{B,k}^T \boldsymbol{\Phi}_{B,k} \boldsymbol{h}_{B,k}$. It is noteworthy that R_i is a function of $\angle\phi_{i,c,n}$ for $n \in \{1, \ldots, N\}$ that is the desired phase shift input for the center frequency f_0.

Because it is intractable to optimize jointly all desired phase control inputs ($\angle\phi_{i,c,n}$'s) for N RIS elements, we adopt a sequential optimization strategy. At each step, we fix all the other phase control inputs and optimize only n th element, $\angle\phi_{i,c,n}$. Therefore, the optimal phase control input ($\angle\phi^*_{i,c,n}$) of the nth element for each RIS can be shown as

$$\angle\phi^*_{i,c,n} = \arg\max_{\angle\phi_{i,c,n}} \frac{1}{K}\sum_{k=1}^{K}\log_2\left(1+\frac{P_i\left|H_{i,k}\right|^2}{\sigma^2}\right). \tag{24}$$

We can derive the closed-form expression of the solution to (24) by following lemma.

Lemma 1: The optimal phase input $\angle\phi^\star_{i,c,n}$ for $i \in \{A, B\}$ that solves the maximization problem in (24) is obtained at a stationary point of $R_i(\angle\phi_{i,c,n})$ over $(-\pi, \pi)$, i.e.,

$$\mathcal{T}_{i,n} = \left\{\angle\phi_{i,c,n}\middle|\frac{dR_i}{d\angle\phi_{i,c,n}} = 0\right\}. \tag{25}$$

If there exist multiple stationary points, we can select the optimal solution maximizing R_i in $\mathcal{T}_{i,n}$.

Proof: The objective function R_i is compositions of smooth functions and squared modulus. Hence, it is continuously differentiable with respect to $\angle\phi_{i,c,n}$. Because the optimization problem in (24) is one–dimensional over the interval $(-\pi, \pi)$, any interior maximizer must satisfy the first-order condition stated above. Since multiple stationary points may exist, boundary points are explicitly compared by direct substitution. The detailed derivative expressions are derived below.

In the objective function in (24), by setting $\alpha_i = \frac{P_i}{\sigma^2}$, $a_{i,k,n} = g_{i,k,n}h_{i,k,n}$, we can express

$$H_{i,k}(\angle\phi_{i,c,n}) = \sum_{n=1}^{N} a_{i,k,n}A_{i,k,n}e^{j\theta_{i,k,n}} \tag{26}$$

$$= a_{i,k,n}A_{i,k,n}e^{j\theta_{i,k,n}} + H_{i,k}^{(-n)}. \tag{27}$$

where $H_{i,k}^{(-n)} \triangleq \sum_{n\neq m} a_{i,k,n}A_{i,k,n}e^{j\theta_{i,k,n}}$. Then, R_i in (23) can be rewritten as

$$R_i(\angle\phi_{i,c,n}) = \frac{1}{K}\sum_{k=1}^{K}\log_2\left(1+\alpha_i|H_{i,k}^{(-n)} + a_{i,k,n}\phi_{i,k,n}|^2\right). \tag{28}$$

Since the above equation is continuously differentiable with $\angle\phi_{i,c,n}$, it's derivative can be readily obtained.

$$\frac{d\ R_i(\angle\phi_{i,c,n})}{d\ \angle\phi_{i,c,n}} = \frac{1}{K\ln 2}\sum_{k=1}^{K}\frac{2\alpha_i}{1+\alpha_i|H_{i,k}|^2}\times \Re\left\{\bar{H}_{i,k}a_{i,k,n}e^{j\theta_{i,k,n}}\left(\frac{\partial A_{i,k,n}}{\partial\angle\phi_{i,c,n}} + jA_{i,k,n}\frac{\partial\theta_{i,k,n}}{\partial\angle\phi_{i,c,n}}\right)\right\} \tag{29}$$

where $\bar{H}_{i,k}$ denotes the complex conjugate of $H_{i,k}$.

Finally, we need to find the closed-form expressions of $\frac{\partial A_{i,k,n}}{\partial\angle\phi_{i,c,n}}$ and $\frac{\partial\theta_{i,k,n}}{\partial\angle\phi_{i,c,n}}$. For any fixed subcarrier k, the functions $A_{i,n,k}(\angle\phi_{i,c,n}, f_k)$ and $\theta_{i,k,n}(\angle\phi_{i,c,n}, f_k)$ are continuously differentiable with respect to $\angle\phi_{i,c,n}$ on $(-\pi, \pi)$. We consider the derivative of amplitude. By using the substitution $\mu \triangleq \frac{f_k - \mathcal{F}_1(\angle\phi_{A,c,n})}{0.05}$, we can rewrite the amplitude of the nth element of RIS_i as

$$A_{i,k,n} = -\frac{\alpha_4\angle\phi_{i,c,n} + \beta_3}{\mu^2+4} + 1 \tag{30}$$

Letting $D \triangleq \mu^2 + 4$, we obtain

$$A_{i,k,n} = -\frac{\alpha_4\angle\phi_{i,c,n} + \beta_3}{D} + 1 \tag{31}$$

By applying the chain rule, the derivative of $A_{i,k,n}$ with respect to $\angle\phi_{i,c,n}$ is given by

$$\frac{\partial A_{i,k,n}}{\partial \angle\phi_{i,c,n}} = -\frac{\alpha_4}{D} + \frac{\alpha_4 \angle\phi_{i,c,n} + \beta_3}{D^2}\left(\frac{2\mu}{0.05}\,\mathcal{F}_1'(\angle\phi_{i,c,n})\right) \quad (32)$$

where $\mathcal{F}_1'$ denotes the derivative of $\mathcal{F}_1$ with respect to $\angle\phi_{i,c,n}$. Next, we consider the derivative of phase. Using the substitution $\omega \triangleq \mathcal{F}_2\big(\angle\phi_{i,c,n}\big)\left(\frac{f_k}{10^9} - \mathcal{F}_1\big(\angle\phi_{i,c,n}\big)\right)$, we can rewrite the phase of nth element of RIS_A as

$$\theta_{i,k,n} = -2\arctan(\omega). \quad (33)$$

By applying the chain rule, the derivative of $\theta_{i,k,n}$ with respect to $\angle\phi_{i,c,n}$ is given by

$$\frac{\partial \theta_{i,k,n}}{\partial \angle\phi_{i,c,n}} = \frac{-2\,\omega'}{1+\omega^2}. \quad (34)$$

where ω' denotes the derivative of ω with respect to $\angle\phi_{i,c,n}$. Expanding ω' and using the definition of $\mathcal{F}_2'$, we obtain

$$\begin{aligned}\frac{\partial \theta_{i,k,n}}{\partial \angle\phi_{i,c,n}} = \frac{-2}{1+\omega^2}\Big(&\alpha_3\big(f_k - \mathcal{F}_1(\angle\phi_{i,c,n})\big) \\ &- \mathcal{F}_2(\angle\phi_{i,c,n})\,\mathcal{F}_1'(\angle\phi_{i,c,n})\Big).\end{aligned} \quad (35)$$

■

Please note that the closed-form expression of $\angle\phi_{i,c,n}$ satisfying $\frac{dR_i}{d\angle\phi_{i,c,n}} = 0$ is obtained by (29) with substitutions of (35) and (32).

To consider practical operations with finite bandwidth of RIS control links between BSs and RISs, the optimized continuous phase shift based on Lemma 1 is then quantized to the nearest entry in the predefined code-book $\mathcal{S} \triangleq \left\{\frac{2\pi}{2^B}b - \pi \,\middle|\, b = 0,\ldots,2^B-1\right\}$ for all $n \in \{1,\ldots,N\}$.

The quantized RIS phase control input for the nth RIS element with Lemma 1 and quantization process is not a joint optimal solution maximizing R_i because this is obtained by (24). To find a joint optimal solution $\{\angle\phi^{\star}_{i,c,n},\ n = 1,\ldots,N\}$, we adopt the alternating optimization approach where the optimization with respect to a single RIS element given by (24) is performed sequentially for $n = 1, 2, \ldots, N$ while all other elements are kept at their current values. The detailed steps are summarized in Algorithm 1. Here, $\widehat{\phi}_{i,c,n}$ is the quantized phase of $\phi^{*}_{i,c,n}$

Algorithm 1 Proposed selfish RIS optimization algorithm.

Initialize $\angle\phi_{i,c,n}$ for $n = \{1,\ldots,N\}$ as zero.
for $iter = 1$ to I_{max} **do**
  for $n = 1$ to N (RIS element index) **do**
    for $k = 1$ to K (subcarrier index) **do**
      $\phi_{i,k,n} = A_{i,k,n}(\angle\phi_{i,c,n}, f_k)e^{j\theta_{i,k,n}(\angle\phi_{i,c,n}, f_k)}$
    end for
  end for
  for $n = 1$ to N (RIS element index) **do**
    Find $\angle\phi^{\star}_{i,c,n}$ with Lemma 1.
    $\widehat{\phi}_{i,c,n} \leftarrow \arg\min_{s\in\mathcal{S}} \left|(\phi^{\star}_{i,c,n} - s)\right|$
    $\angle\phi_{i,c,n} \leftarrow \widehat{\phi}_{i,c,n}$
  end for
end for

B. Case-2: Cross-RIS-aware RIS Control

In Case-2, the effects of the neighboring RIS are also taken into account in the optimization of RIS phase shift. To this end, two BSs (BS_A and BS_B) cooperate and maximize the sum achievable rates of UEs. The average achievable rate of UE_i is defined as

$$R_i' \triangleq \frac{1}{K}\sum_{k=1}^{K}\log_2\left(1 + \frac{P_i\,|H_i + G_i|^2}{\sigma^2}\right) \quad (36)$$

where the effective channel gain from BS_i to UE_i via the other cell RIS, $RIS_{j,j\neq i}$, is defined by G_i. Therefore, G_i's for $i \in \{A, B\}$ are given by $G_A \triangleq \boldsymbol{k}_{B,k}^T\,\boldsymbol{\Phi}_{B,k}\,\boldsymbol{c}_{A,k}$ and $G_B \triangleq \boldsymbol{k}_{A,k}^T\,\boldsymbol{\Phi}_{A,k}\,\boldsymbol{c}_{B,k}$. The joint optimization problem maximizing the sum rates by adjusting the phase shift of both RISs can be formulated as follows:

$$\left(\angle\phi^{\star}_{A,c,n},\ \angle\phi^{\star}_{B,c,n}\right) = \arg\max_{\angle\phi_{A,c,n}\ \angle\phi_{B,c,n}} (R_A' + R_B') \quad (37)$$

Optimization of the two variables is difficult to solve. We solve the problem by BCA algorithm, alternately updating $\angle\phi_{A,c,n}$ and $\angle\phi_{B,c,n}$ until convergence. Similar to Lemma 1, the objective function R_i' involves two variables $\angle\phi_{A,c,n}$ and $\angle\phi_{B,c,n}$. We first fix $\angle\phi_{B,c,n}$ for all elements n, and differentiate R_i' with respect to $\angle\phi_{A,c,n}$ to obtain its optimal value for all elements n. And then keep $\angle\phi_{A,c,n}$ fixed for all elements n, while optimizing R_i' with respect to $\angle\phi_{B,c,n}$. The optimal phase control input $\left(\angle\phi^{\star}_{A,c,n}, \angle\phi^{\star}_{B,c,n}\right)$ that solves the maximization problem in (37) is obtained at a stationary point of $R_i'(\angle\phi_{A,c,n}, \angle\phi_{B,c,n})$ over $(-\pi, \pi)$, i.e.,

$$\angle\phi^{\star}_{A,c,n} = \left\{\angle\phi_{A,c,n} \,\middle|\, \frac{\partial R_i'(\angle\phi_{A,c,n}, \angle\phi_{B,c,n})}{\partial\angle\phi_{A,c,n}} = 0\right\}, \quad (38)$$

$$\angle\phi^{\star}_{B,c,n} = \left\{\angle\phi_{B,c,n} \,\middle|\, \frac{\partial R_i'(\angle\phi^{\star}_{A,c,n}, \angle\phi_{B,c,n})}{\partial\angle\phi_{B,c,n}} = 0\right\}. \quad (39)$$

Following a similar procedure as in the proof of lemma 1, we can rewrite the objective function in (36). By setting $b_{A,k,n} = k_{B,k,n}c_{A,k,n}$ and $b_{B,k,n} = k_{A,k,n}c_{B,k,n}$, we can express as

$$G_{A,k}(\angle\phi_{B,c,n}) = \sum_{n=1}^{N} b_{A,k,n}A_{B,k,n}e^{j\theta_{B,k,n}} \quad (40)$$

$$= b_{A,k,n}A_{B,k,n}e^{j\theta_{B,k,n}} + G_{A,k}^{(-n)}, \quad (41)$$

$$G_{B,k}(\angle\phi_{A,c,n}) = \sum_{n=1}^{N} b_{B,k,n}A_{A,k,n}e^{j\theta_{A,k,n}} \quad (42)$$

$$= b_{B,k,n}A_{A,k,n}e^{j\theta_{A,k,n}} + G_{B,k}^{(-n)}. \quad (43)$$

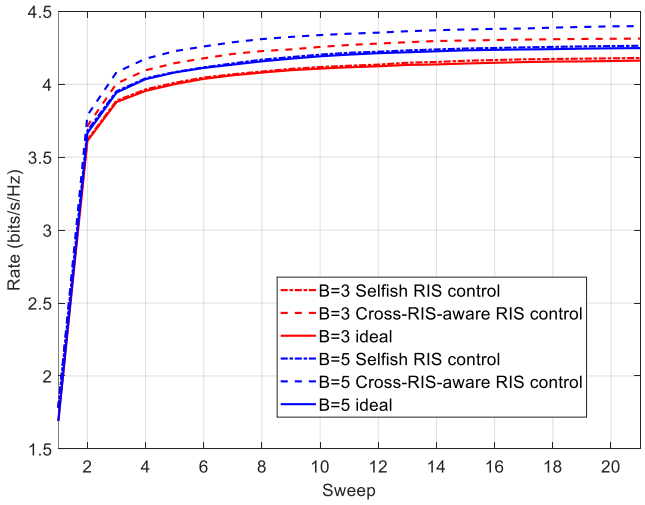

Fig. 2. Average sum rate over sweeps for different codebook sizes under each case.

where $G_{A,k}^{(-n)} \triangleq \sum_{n\neq m} b_{A,k,n}A_{B,k,n}e^{j\theta_{B,k,n}}$, and $G_{B,k}^{(-n)} \triangleq \sum_{n\neq m} b_{B,k,n}A_{A,k,n}e^{j\theta_{A,k,n}}$. Then, R'_A and R'_B in (37) can be rewritten as

$$R'_A(\angle\phi_{A,c,n}, \angle\phi_{B,c,n}) = \frac{1}{K}\sum_{k=1}^{K}\log_2\Big(1+\alpha_A\big|H_{A,k}^{(-n)} + G_{A,k}^{(-n)} + a_{A,k,n}\phi_{A,k,n} + b_{A,k,n}\phi_{B,k,n}\big|^2\Big). \tag{44}$$

$$R'_B(\angle\phi_{A,c,n}, \angle\phi_{B,c,n}) = \frac{1}{K}\sum_{k=1}^{K}\log_2\Big(1+\alpha_B\big|H_{B,k}^{(-n)} + G_{B,k}^{(-n)} + a_{B,k,n}\phi_{B,k,n} + b_{B,k,n}\phi_{A,k,n}\big|^2\Big). \tag{45}$$

Since both equations are continuously differentiable with respect to $\angle\phi_{i,c,n}$, the object function in (37) is also differentiable. It's derivative can be obtained in a similar manner as in Lemma (1). The cross-RIS-aware optimization follows a similar procedure with Algorithm 1, but it involves a joint objective function $R'_A+R'_B$ with respect to two coupled variables. To solve this, we adopt an alternating optimization strategy. Specifically, the phase shifts of all elements in RIS_A are first optimized by taking the partial derivative of the sum rate with respect to $\angle\phi_{A,c,n}$, while keeping RIS_B fixed. Then, with the updated RIS_A, the optimal phase shifts $\angle\phi_{B,c,n}$ for RIS_B are obtained in a similar manner. This process is repeated until convergence. Due to space constraints, the detailed discussion of the optimal solution and algorithm is omitted.

IV. Simulation Results

We considered a two cell RIS–aided downlink in which the two base stations operate on different center frequencies, i.e., BS_A at 2.4 GHz and BS_B at 2.5 GHz. The channel bandwidth is 100 MHz with $K = 64$ subcarriers. Each cell uses an RIS with $N = 128$ reflecting elements. All RIS elements are sequentially updated from $N = 1$ to $N = 128$, with the current optimal phase applied at each step. Because later updates can change the optimality of earlier elements, the phase chosen for previous one may no longer be optimal after the end of update. Even in the selfish-RIS design considering an own-cell RIS path only, the actual achievable rate is obtained with both own-cell and other-cell RIS paths. Hence, we plot $R_{\text{sum}} = \frac{1}{2}\left(R'_A + R'_B\right)$ versus the number of sweeps to verify convergence. Fig. 2 illustrates the convergence behavior of the proposed algorithm, where the sum rate is averaged over 50 independent channel realizations. It can be observed that the Rate monotonically increases with the number of sweeps and reaches a stable value after around 16 sweeps. The initial value is obtained from the zero-phase initialization. For comparison, we also introduce an ideal case for each value of B. In this ideal case, the phase shifts are optimized in the same way as in Case 1, but when computing the sum rate, we ignore the paths reflected by the other-cell RIS and only account for the contributions from the serving RIS. As shown in Fig. 2, The cross–RIS-aware design (Case-2), which sets phases while accounting for neighboring RIS, consistently outperforms the selfish–RIS design (Case-1). The final rate gap between Case-2 and Case-1 is small, about 0.1328 and 0.1348 bits/s/Hz for $B = 3, B = 5$ respectively. In addition, as observed in [15], the ideal case yields a lower rate than Case 1. This confirms that the additional paths created by the other-cell RIS are responsible for the performance gain. The differences between the sizes of the quantization code-book B were marginal. Although large B yields a slightly higher converged rate, the differences were not statistically significant.

V. Conclusion

In this paper, we proposed a new formulation of the RIS phase-shift design problem in RIS-aided multiuser systems. Under this formulation, we solve the optimization problem via block coordinate ascent (BCA). Our simulation results show that the proposed model achieves a higher average rate than the baseline models. Varying the code-book size within $B \in \{3, 4, 5\}$ yields only a modest impact on the achievable rate. Also, compared to the ideal case which neglects the contributions from cross-RIS paths, both of case-1 and case-2 achieve higher average sum rats. It should be noted that the proposed cross-RIS-aware RIS control requires cooperation between base stations, which involves the sharing of CSI. While prior work [17] indicates that the overhead associated with transmitter cooperation may outweigh the achievable gains, the considered scenarios are fundamentally different from the one addressed in this paper. Therefore, further investigation is required to determine whether the performance gains provided by the proposed approach can justify the additional cooperation overhead in the considered system.

Acknowledgment

This work was supported by the National Research Foundation of Korea(NRF) grant funded by the Korea govern-

ment(MSIT) (RS-2025-00514779, RS-2025-02303435).

References

[1] M. Shahjalal *et al.*, "Enabling technologies for AI-empowered 6G massive radio access networks," *ICT Express*, vol. 9, no. 3, pp. 341–355, Jun. 2023.

[2] W. Khalid, A. -A. A. Boulogeorgos, T. Van Chien, J. Lee, H. Lee, and H. Yu, "Optimal operation of active RIS-aided wireless powered communications in IoT networks," *IEEE Internet Things J.*, vol. 12, no. 1, pp. 390–401, Jan. 2025.

[3] S. Noh, K. Seo, Y. Sung, D. J. Love, J. Lee, and H. Yu, "Joint direct and indirect channel estimation for RIS-assisted millimeter-wave systems based on array signal processing," *IEEE Trans. Wirel. Commun.*, vol. 22, no. 11, pp. 8378–8391, Nov. 2023.

[4] S. Noh, J. Lee, G. Lee, K. Seo, Y. Sung, and H. Yu, "Channel estimation techniques for RIS-assisted communication: Millimeter-wave and sub-THz systems," *IEEE Veh. Technol. Mag.*, vol 17, no. 2, pp. 64–73, Jun. 2022.

[5] W. Kalid, T. V. Chien, W. U. Khan, Z. Kaleem, Y. B. Zikria, T. Kim, and H. Yu, "Malicious Reconfigurable Intelligent Surfaces: Security Threats in 6G Networks," *IEEE Internet Things J.*, vol. 12, no. 15, pp. 30063-30085, Aug. 2025.

[6] W. Khalid, Z. Kaleem, R. Ullah, T. V. Chien, S. Noh, and H. Yu, "Simultaneous transmitting and reflecting-reconfigurable intelligent surface in 6G: Design guidelines and future perspectives," *IEEE Netw.*, vol. 37, no. 5, pp. 173–181, Dec. 2022.

[7] W. Khalid, H. Yu, D. -T. Do, Z. Kaleem, and S. Noh, "RIS-aided physical layer security with full-duplex jamming in underlay D2D networks," *IEEE Access*, vol. 9, pp. 99667–99679, Jul. 2021.

[8] J. Bae, W. Khalid, A. Lee, H. Lee, S. Noh, and H. Yu, "Overview of RIS-enabled secure transmission in 6G wireless networks," *Digit. Commun. Netw.*, vol. 10, no. 6, pp. 1553–1565, Dec. 2024.

[9] W. Khalid, H. Yu, and A. -A. A. Boulogeorgos, "Outage analysis for active reconfigurable intelligent surface-enhanced wireless powered communication networks," in *Proc. IEEE Int. Conf. Artif. Intel. Inf. Commun. (ICAIIC)*, Osaka, Japan, 19-22 Feb. 2024.

[10] M. R. A. Ruku, M. Ibrahim, A. S. M. Badrudduza, I. S. Ansari, W. Khalid, and H. Yu, "Effects of co-channel interference on RIS empowered wireless networks amid multiple eavesdropping attempts," *ICT Express*, vol. 10, no. 3, pp. 491–497, Jun. 2024.

[11] W. Khalid, M. A. U. Rehman, T. Van Chien, Z. Kaleem, H. Lee, and H. Yu, "Reconfigurable intelligent surface for physical layer security in 6G-IoT: Designs, issues, and advances," *IEEE Internet Things J.*, vol. 11, no. 2, pp. 3599–3613, Jan. 2024.

[12] C. Huang, A. Zappone, G. C. Alexandropoulos, M. Debbah and C. Yuen, "Reconfigurable Intelligent Surfaces for Energy Efficiency in Wireless Communication," *IEEE Trans. Wirel. Commun.*, vol. 18, no. 8, pp. 4157-4170, Aug. 2019.

[13] Q. Wu, S. Zhang, B. Zheng, C. You and R. Zhang, "Intelligent Reflecting Surface-Aided Wireless Communications: A Tutorial," *IEEE Trans. Commun.*, vol. 69, no. 5, pp. 3313-3351, May 2021.

[14] Y. Yang, B. Zheng, S. Zhang and R. Zhang, "Intelligent Reflecting Surface Meets OFDM: Protocol Design and Rate Maximization," *IEEE Trans. Commun.*, vol. 68, no. 7, pp. 4522-4535, July 2020.

[15] L. Yashvanth and C. R. Murthy, "On the Impact of an IRS on the Out-of-Band Performance in Sub-6 GHz and mmWave Frequencies," *IEEE Trans. Commun.*, vol. 72, no. 12, pp. 7417-7434, Dec. 2024.

[16] W. Cai, H. Li, M. Li and Q. Liu, "Practical Modeling and Beamforming for Intelligent Reflecting Surface Aided Wideband Systems," *IEEE Commun. Lett.*, vol. 24, no. 7, pp. 1568-1571, July 2020.

[17] A. Zappone, M. Di Renzo, F. Shams, X. Qian and M. Debbah, "Overhead-Aware Design of Reconfigurable Intelligent Surfaces in Smart Radio Environments," *IEEE Trans. Commun.*, vol. 20, no. 1, pp. 126-141, Jan 2021.